

Nanoplasmonic Renormalization and Enhancement of Coulomb Interactions

Maxim Durach,¹ Anastasia Rusina,¹ Victor I. Klimov,² and Mark I. Stockman¹

¹ *Department of Physics and Astronomy, Georgia State University, Atlanta, Georgia 30303, USA*

² *Chemistry Division, C-PCS, Los Alamos National Laboratory, Los Alamos, New Mexico 87545, USA*

(Dated: October 29, 2018)

Nanostructured plasmonic metal systems are known to enhance greatly variety of radiative and nonradiative optical processes, both linear and nonlinear, which are due to the interaction of an electron in a molecule or semiconductor with the enhanced local optical field of the surface plasmons. Among them are surface enhanced Raman scattering (SERS)^{1,2,3,4,5,6}, surface plasmon enhanced fluorescence^{5,7,8,9,10,11}, fluorescence quenching in the proximity of metal surfaces,^{7,10,12} coherent anti-Stokes Raman scattering (CARS)¹³, surface enhanced hyper-Raman scattering (SEHRS)¹⁴, etc. Principally different are numerous many-body phenomena that are due to the Coulomb interaction between charged particles: carriers (electrons and holes) and ions. These include carrier-carrier or carrier-ion scattering, energy and momentum transfer (including the drag effect), thermal equilibration, exciton formation, impact ionization, Auger effects,¹⁵ etc. It is not widely recognized that these and other many-body effects can also be modified and enhanced by the surface-plasmon local fields. A special but extremely important class of such many-body phenomena is constituted by chemical reactions at metal surfaces, including catalytic reactions. Here, we propose a general and powerful theory of the plasmonic enhancement of the many-body phenomena resulting in a closed expression for the surface plasmon-dressed Coulomb interaction. We illustrate this theory by computing this dressed interaction explicitly for an important example of metal-dielectric nanoshells,¹⁶ which exhibits a reach resonant behavior in both the magnitude and phase. This interaction is used to describe the nanoplasmonic-enhanced Förster energy transfer between nanocrystal quantum dots in the proximity of a plasmonic nanoshell. This is of great interest for plasmonic-enhanced solar cells and light-emitting devices.¹⁷ Catalysis at nanostructured metal surfaces, nonlocal carrier scattering, and surface-enhanced Raman scattering are discussed among other effects and applications where the nanoplasmonic renormalization of the Coulomb interaction may be of principal importance.

PACS numbers: 78.67.-n, 71.45.Gm, 73.20.Mf

Consider a system of charged particles situated in the vicinity of a plasmonic metal nanosystem. For definiteness, we will assume that these particles are electrons, although they can also be holes or ions of the lattice. One of the examples of such systems is a semiconductor in the proximity of a nanostructured metal surface. When an electron undergoes a transition with some frequency ω , this transition is accompanied by local electric fields oscillating with the same frequency. These fields excite surface plasmon (SP) modes with the corresponding frequencies whose fields overlap in space with the transition fields. A property of these SP eigenmodes is that they can be delocalized over the entire nanostructure¹⁸. The local optical fields of the SPs can excite a resonant transition of another electron. This process, which in the quantum-mechanical language is the electron-electron interaction by the exchange of a SP quantum, renormalizes (“dresses”) the direct interaction between these two charges. As a result, the direct (“bare”) Coulomb interaction between the electrons, $V(\mathbf{r} - \mathbf{r}') = 1/(\epsilon_h |\mathbf{r} - \mathbf{r}'|)$, where ϵ_h is the dielectric constant of the embedding medium, is replaced by the dressed interaction $W(\mathbf{r}, \mathbf{r}'; \omega)$. This dressed interaction is generally not translationally-invariant, i.e., it depends on coordinates \mathbf{r} and \mathbf{r}' of both electrons; it also depends on the transition frequency ω . Note that W is generally a complex function, and its phase describes a delay inherent in the plasmonic reaction. This phase varies sharply across plasmonic resonances, as we will show later in this Letter.

We schematically illustrate this SP-mediated electron-electron interaction in Fig. 1 where we show electrons in two semiconductor nanocrystal quantum dots (NQDs) situated at the surface of a metal nanostructure. The plasmonic fields, indicated by orange, excited by one of the electrons interact with the other one in a different NQD. The interacting charges could also belong to the same quantum dot and could be not only electrons but also holes.

The resonant nature of the electron-plasmon interaction may lead to the significant enhancement of the dressed interaction W with respect to the bare one, V . A typical SP eigenmode tends to form “hot spots” of the local fields separated by distances on the order of the size of the entire plasmonic nanostructure¹⁸. Therefore one should expect that the dressed interaction will also be delocalized over such distances, i.e., be much more long-ranged than the bare Coulomb interaction.

The dressed interaction $W(\mathbf{r}, \mathbf{r}'; \omega)$, by definition, is the potential created at a point \mathbf{r} by a charge positioned at another point \mathbf{r}' and oscillating with frequency ω . We assume that the size of the system is much smaller than any relevant electromagnetic length (radiation wavelength, skin depth, etc.) and will use the quasistatic approximation,

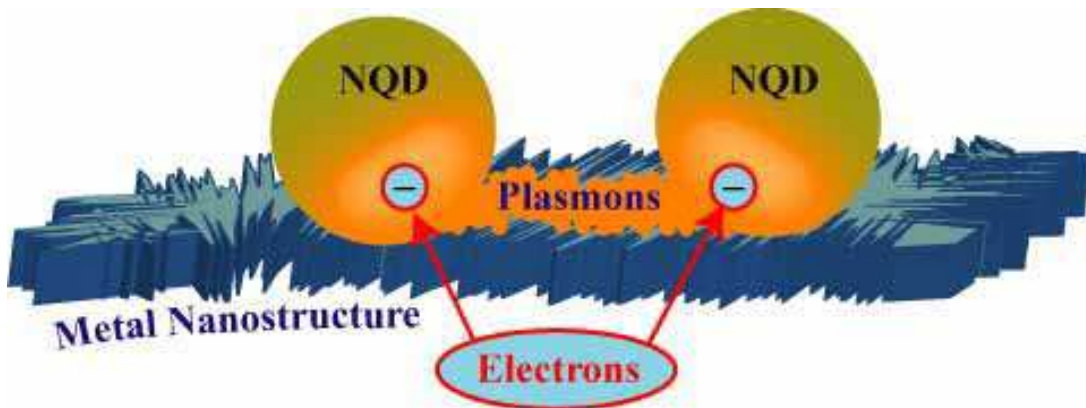


FIG. 1: Schematic of metal nanostructure and semiconductor nanocrystal quantum dots (NQDs) situated in its vicinity. The metal nanostructure is depicted by the dark blue color. Two electrons are indicated in NQDs by the blue color and the local plasmonic fields are schematically shown by the orange color.

which is conventional in nanoplasmonics. In this case, W satisfies the continuity equation

$$\frac{\partial}{\partial \mathbf{r}} \left[\varepsilon(\mathbf{r}, \omega) \frac{\partial}{\partial \mathbf{r}} W(\mathbf{r}, \mathbf{r}'; \omega) \right] = -4\pi\delta(\mathbf{r} - \mathbf{r}') , \quad (1)$$

where dielectric function of the system $\varepsilon(\mathbf{r}, \omega)$ is expressed as $\varepsilon(\mathbf{r}, \omega) = \varepsilon_m(\omega)\Theta(\mathbf{r}) + \varepsilon_h[1 - \Theta(\mathbf{r})]$. Here, $\Theta(\mathbf{r})$ is the characteristic function equal to 1 when \mathbf{r} belongs to the metal and 0 otherwise, and $\varepsilon_m(\omega)$ is the dielectric function of the uniform metal.

A general solution to this equation can be written in terms of the retarded Green's function of the system G^r as

$$W(\mathbf{r}, \mathbf{r}'; \omega) = V(\mathbf{r} - \mathbf{r}') - \int V(\mathbf{r}'' - \mathbf{r}') \frac{\partial^2}{\partial \mathbf{r}''^2} G^r(\mathbf{r}, \mathbf{r}''; \omega) d^3 r'' . \quad (2)$$

In Methods Section, we follow theory^{19,20} to outline derivation and properties of G^r , which can be presented as a spectral expansion over SP eigenmodes $\varphi_n(\mathbf{r})$ and the corresponding eigenvalues s_n as

$$G^r(\mathbf{r}, \mathbf{r}'; \omega) = \sum_n \frac{s_n}{s(\omega) - s_n} \varphi_n(\mathbf{r}) \varphi_n(\mathbf{r}') , \quad (3)$$

where $s(\omega) = 1/[1 - \varepsilon_m(\omega)/\varepsilon_d]$ is the spectral parameter. If the system is in an infinite space (or the boundaries are remote enough), then the use of Green's identity in Eq. (2) simplifies it to the form

$$W(\mathbf{r}, \mathbf{r}'; \omega) = V(\mathbf{r} - \mathbf{r}') + \frac{4\pi}{\varepsilon_h} G^r(\mathbf{r}, \mathbf{r}'; \omega) . \quad (4)$$

This is a simple, yet, general and powerful result: the Coulomb interaction is renormalized by the full retarded Green's function whose contraction also describes the nanoplasmonic enhancement of SERS⁶ and other optical phenomena. The poles of Green's function (3) correspond to the SP modes whose frequencies ω_n are given by the equation $s(\omega_n) = s_n$. Close to such a frequency, G^r becomes large, proportional to the quality factor Q_n of the SP resonance.⁶ This describes the plasmonic renormalization and enhancement of the dressed Coulomb interaction.

We will illustrate the plasmonic renormalization and enhancement of the Coulomb interaction using a metal nanoshell as a nanoplasmonic system. Such nanoshells have significant fundamental and applied interest.¹⁶ For nanoshells, the renormalized Coulomb interaction is derived in Methods as Eq. (14). We depict the resonant behavior and renormalization (enhancement) of the Coulomb interaction in Fig. 2 for a silver nanoshell with aspect ratio $x = 0.9$ deposited on a dielectric core with permittivity $\varepsilon_h = 2$ embedded into a host with the same permittivity. Silver dielectric function is adopted from the experimental data.²¹ For this specific nanoshell, the lowest dipole eigenmode (quantum numbers $L = 1, P = -$) has eigenfrequency $\hbar\omega_{1-} = 1.60$ eV. For a red-detuned (from the dipole SP resonance) electronic transition frequency $\hbar\omega = 1.5$ eV, the renormalized interaction is displayed in Fig. 2(a). Very close to the singular point $\mathbf{r} = \mathbf{r}'$, the renormalization is reduced to conventional dielectric screening: this is displayed by the opposite sign (blue color in the panel) of $\text{Re} W(\mathbf{r}, \mathbf{r}'; \omega)$ with respect to the bare Coulomb potential (the red dot pointed to by the arrow). On the opposite side of the nanosphere, there is a "mirror image" of the

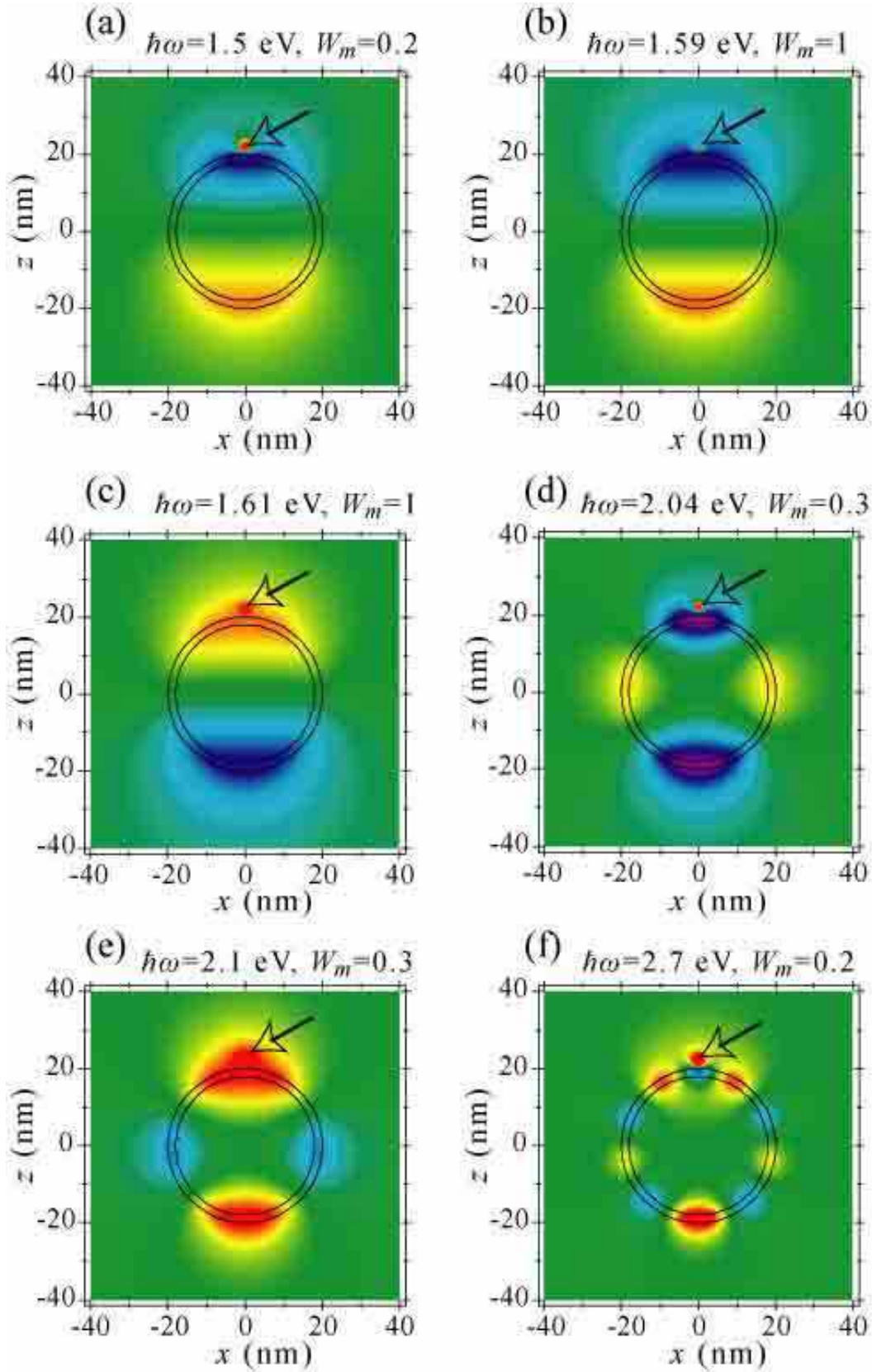


FIG. 2: Renormalized (dressed) Coulomb interaction $\text{Re } W(\mathbf{r}, \mathbf{r}'; \omega)$ for silver nanoshell of aspect ratio $x = 0.9$. Point \mathbf{r}' is fixed and indicated by the black arrows in the upper parts of the panels. The dependence of $\text{Re } W(\mathbf{r}, \mathbf{r}')$ on $\mathbf{r} = \{x, z\}$ is shown by color coding in the panels for the cross section of the shell. The limits of this color coding are $\pm W_m$; the maximum W_m and higher values of $\text{Re } W$ are depicted by red, and the minimum $-W_m$ and lower values of $\text{Re } W$ are shown by blue. Frequencies ω are indicated in the panels.

dressed interaction potential $\text{Re}W$ oscillating in phase (as indicated by the red color) with the initial field. This shows that the nanoplasmonic effects greatly extend the range of the dressed Coulomb interaction. This is due to the delocalization the dipole eigenmode, which defines the nanoplasmonic effects in this spectral region.

For $\hbar\omega = 1.59$ eV, which is very close to (but still red-detuned from) the dipole SP resonance, the real part of the renormalized Coulomb interaction potential, $\text{Re}W(\mathbf{r}, \mathbf{r}'; \omega)$ is displayed in Fig. 2(b). In this case, the dynamic screening of the bare potential becomes very strong, which is seen from the diminished magnitude and radius of the Coulomb potential shown as the small red dot pointed by the arrow. The W interaction, however, is strongly delocalized both around the point \mathbf{r}' where the charge is situated (manifested by the intense blue “cloud”) and at the opposite pole of the nanoshell where the sign of the interaction is the same as that for the bare charge (red color).

The situation changes dramatically for a frequency $\hbar\omega = 1.61$ eV, which is slightly above the dipole resonant frequency – see Fig. 2(c). In this case, the SP renormalization is actually dynamic *anti*-screening: both the radius and strength of the Coulomb interaction in the vicinity of the initial charge are increased. The renormalized potential oscillates in phase with the bare Coulomb potential, as indicated by the red color of the cloud around the arrow. There is also a very strong interaction potential on the diametrically opposite side of the nanoshell, which oscillates out of phase (shown by blue). Thus, close to but slightly blue-detuned from the SP resonance, the dressed (renormalized) potential for \mathbf{r} in the vicinity of \mathbf{r}' becomes very large, which can be described as the nanoplasmonic enhancement due to the dynamic antiscreening.

As frequency ω increases further [Fig. 2 (d)-(f)], higher-multipole SP eigenmodes start to contribute to the Coulomb potential dressing, starting with the quadrupole in panels (d) and (e). In all the cases, the screening in the vicinity of the charge for frequencies to the red of the resonance changes to the antiscreening for blue spectral detuning. The dressed potential is delocalized over the surface of the nanoshell, thus becoming extremely long-ranged. This is a general property of the nanoplasmonic renormalization of the Coulomb interaction: the range of the dressed interaction always extends over the entire nanoplasmonic system. This effect is due to the absence of the strong localization of the SP eigenmodes, cf. Ref. 18.

In Fig. 2, we have plotted only the real part of the renormalized Coulomb potential $W(\mathbf{r}, \mathbf{r}'; \omega)$. However, its imaginary part (not shown) is also important. In the resonant cases, it is greatly enhanced and delocalized over the entire nanosystem. Because of the underlying $\pi/2$ phase shift, it does not interfere with the real part of W . It always increases the strength and contributes to the delocalization of the dressed interaction.

One of the many-body effects that is affected by the nanoplasmonic renormalization of the Coulomb interaction is the Förster resonant energy transfer (FRET).^{22,23} It has been proposed theoretically^{24,25} and observed experimentally²⁶ that the Förster transfer between chromophores in the proximity of a metal spheroid is enhanced by the SP effect. Note that SP-mediated energy transfer across a metal film has also been observed.²⁷ Below, as an illustration of our general theory, we consider FRET for chromophores at the surface of a metal/dielectric nanoshell. As we have already mentioned, the nanoshells are spectrally tunable and can have their SP eigenmodes shifted by frequency to the red and near-ir spectral regions,¹⁶ which results in increased values of the resonance quality factor due to lower dielectric losses of the metal,²¹ and, hence, enhanced plasmonic effects.

The FRET is an electron-electron interaction (many-body) effect that is due to dipole electronic transitions. It is described by Hamiltonian that is a dipolar expansion of interaction (4):

$$H'_{\text{FRET}} = \left(\mathbf{d}_d \frac{\partial}{\partial \mathbf{r}} \right) \left(\mathbf{d}_a \frac{\partial}{\partial \mathbf{r}'} \right) W(\mathbf{r}, \mathbf{r}'; \omega), \quad (5)$$

where \mathbf{d}_d and \mathbf{d}_a are the dipole operators of the two interacting electrons (the energy donor and acceptor) at points \mathbf{r} and \mathbf{r}' , respectively. Note that the SPs of all multiplicities are taken into account by Eq. (5).

For certainty, we will consider FRET between the electrons belonging to two different NQDs, similarly to what is schematically illustrated in Fig. 1. It is known that the direct (without SP participation) FRET occurs between two NQDs only at very short distances, on the order of just a few nanometers.^{28,29,30} We will be interested in the FRET over larger distances where it occurs predominantly via an SP-mediated process. We assume that the transitions $i \leftrightarrow f$ between the initial and final states in NQDs are unpolarized, i.e., the corresponding transition dipole moments $(\mathbf{d}_d)_{if}$ and $(\mathbf{d}_a)_{if}$ are randomly-oriented vectors. In such a case, substituting Hamiltonian (5) into the Fermi Golden Rule and averaging over the dipole orientations, we obtain an expression for the plasmon-enhanced FRET rate γ_F ,

$$\gamma_F = \frac{2\pi \left| (\mathbf{d}_d)_{if} \right|^2 \left| (\mathbf{d}_a)_{if} \right|^2}{9\hbar^2} \left| W_{\alpha\beta}(\mathbf{r}, \mathbf{r}'; \omega) \right|^2 J, \quad (6)$$

where $\alpha, \beta = x, y, z$ are vector indices (repeated indices imply summation), $W_{\alpha\beta}$ is a dyadic renormalized interaction defined in Methods Section by Eq. (11), and J is the spectral overlap integral. If the energy donor and acceptor transitions $i \leftrightarrow f$ both have Lorentzian shapes with the same central frequency ω (i.e., are resonant) and have homogeneous widths of γ_d and γ_a , then $J = (2/\pi) (\gamma_a + \gamma_d)^{-1}$.

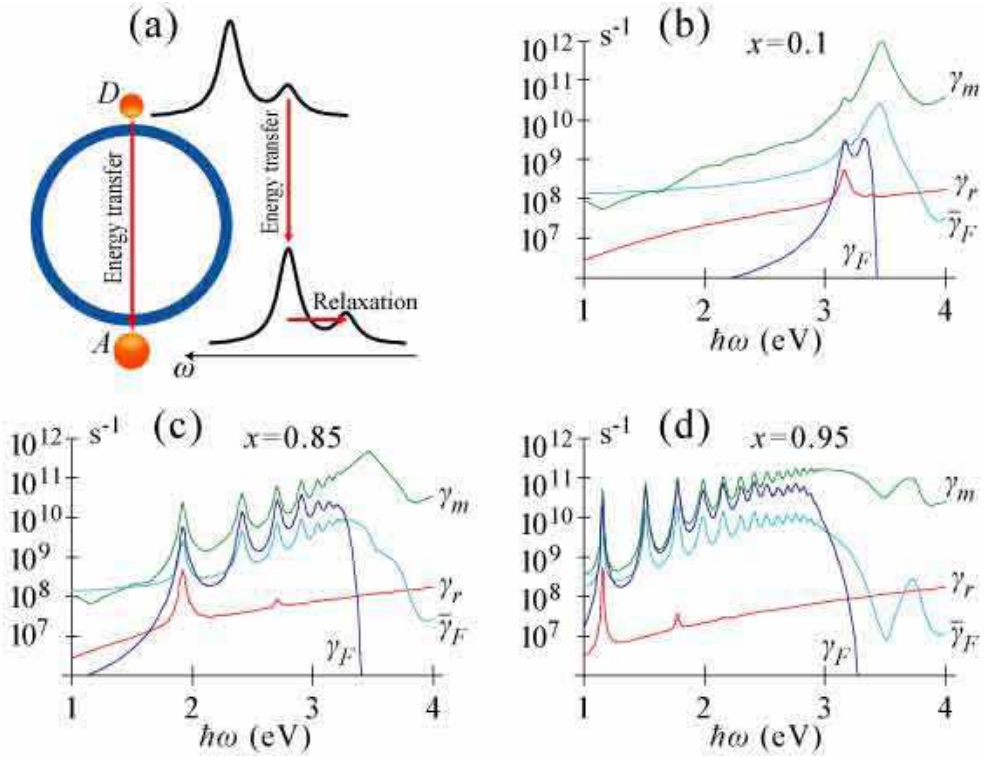


FIG. 3: Transfer and relaxation rates for NQDs at the outer surface of silver nanoshell, modified and enhanced by SPs. (a) Schematic of the system and energy transfer processes. A nanoshell is indicated by a blue circle, and the donor and acceptor NQDs are labelled D and A, correspondingly. The frequency distributions of the transition oscillator strengths of the donor and acceptor NQDs are shown by bold black curves. The energy transfer between NQDs and subsequent relaxation are indicated by red arrows. (b)-(c) The nonradiative and radiative relaxation rates (in the logarithmic scale) for NQDs on nanoshells for the aspect ratios x specified in the panels. The FRET rate γ_F (6) for two NQDs situated on the opposite poles of a nanoshell [cf. panel (a)] is shown by the blue curves. The SP-mediated FRET rate averaged over the position of the acceptor on the nanoshell $\bar{\gamma}_F$ (17) is shown by the light-blue curves. The rate of transfer to the metal γ_m (18) is plotted by the green curves. The radiative rate γ_r (13) for a NQD at the surface of the nanoshell is depicted by the red curves.

We compute the FRET rate for CdSe NQDs that are situated at the surface of a silver nanoshell. For certainty, we further assume that they are positioned at the opposite sides of the nanoshell, as illustrated in Fig. 3 (a). In CdSe NQDs, the lowest-energy, emitting exciton state has a relatively weak oscillator strength and is shifted by a few tens of meV (global Stokes shift) to the red with respect to the stronger absorbing transition [see spectra shown by the bold black lines in Fig. 3(a)]. Because of this significant Stokes shift, the energy transfer occurs with an appreciable efficiency only between NQDs with some size difference, which provides resonant coupling of the emitting state of the donor (the smaller NQD) to the absorbing state of the acceptor (the larger NQD).^{29,30} This process is schematically illustrated in Fig. 3(a).

After the Förster energy transfer, indicated by the vertical red arrow, there is a fast (< 1 ps lifetime) relaxation into the lower-frequency state of the acceptor, which precludes the energy transfer back to the donor and allows one to use the perturbation theory result of Eq. (6) describing an irreversible transfer. We adopted NQD parameters for room temperature from Ref. 29: $J = 0.004$ cm (or, 0.13 ps); $d_a = 25$ Debye, and $d_d = 4.4$ Debye. Note that from this value of J , one can obtain an estimate for the homogeneous width of the donor and acceptor transitions $\gamma_a + \gamma_d = 31$ meV, which implies that these transitions are significantly broadened at room temperature, probably, due to the electron-phonon interaction.

For certainty, we consider nanoshells with the outer radius $a = 20$ nm. The donor and acceptor NQDs are separated by 2 nm from the metal surface. The FRET rates along with the rates of the nonradiative and radiative decays of the NQDs are displayed in Fig. 3 (b)-(d). We show both the FRET rate γ_F (6) for the transfer across the diameter of the nanoshell (dark-blue curves) and the FRET rate $\bar{\gamma}_F$ (17) averaged over the random position of the acceptor on the surface of the NQD (light-blue curves). This averaged rate is calculated and shown per a single acceptor; if several acceptors participate in the energy transfer, this rate should be multiplied by the number of such acceptors on the nanoshell. Also shown by the green curves is rate γ_m (18) of nonradiative relaxation due to the energy transfer

to the metal. The rate the radiative decay γ_r (13) is depicted by the red curves.

For all aspect ratios [Fig. 3 (b)-(d)], the FRET rates γ_F and $\bar{\gamma}_F$ are enhanced at the frequencies of the SP eigenmodes, which is manifested by the corresponding resonant peaks in the graphs. The number of the efficiently contributing multipoles progressively increases from two (dipole and quadrupole) for a low aspect ratio [$x = 0.1$, panel (a)] to very many multipoles for high aspect ratios [$x = 0.85 - 0.95$, panels (c) and (d)]. With increasing aspect ratio x , the corresponding FRET rates in these peaks (at the resonant SP frequencies) become higher by orders of magnitude. Especially large this FRET transfer rate is in the lower-frequency spectral range, which is due to a higher plasmonic quality of the metal.

The transfer to metal is an important process because it competes with FRET. The nonradiative relaxation rate in the donor state of isolated NQDs is low ($< 0.05 \text{ ns}^{-1}$); therefore the energy transfer rate to metal γ_m is the major factor that determines the quantum yield of FRET: $Q_F = \gamma_F / (\gamma_m + \gamma_F)$. We can see from Fig. 3 (b) that for low-aspect ratio nanoshells $\gamma_F \ll \gamma_m$ and, hence, $Q_F \ll 1$ implying that the FRET is inefficient. The FRET of low efficiency was also found for solid nanospheres in Ref. 25. As the aspect ratio increases [panels (c) and (d)], this metal-quenching rate γ_m also shows plasmonic peaks; however, it is enhanced significantly less than the FRET rate. Correspondingly, for $x = 0.95$ the FRET quantum yield is rather high, $Q \sim 0.5$, in the red and near-ir regions of the spectrum. In contrast, the radiative rate γ_r [Eq. (13)] is orders of magnitude lower than γ_m ; correspondingly, the photoemission quantum yield is very low. Note that the radiative rate is enhanced only in the odd-multipole (dipole, octupole, etc.) SP resonances due to the parity selection rule.

The overall conclusion from Fig. 3 is that the SP renormalization of the Coulomb interaction causes a strong enhancement of the Förster transfer at large distances, across the entire nanoshell and over a wide range of frequencies where many multipole SP resonances contribute. This enhancement is especially pronounced for high-aspect ratio nanoshells in the red and near-ir frequency range where rather high FRET efficiency is predicted.

To summarize briefly, significant renormalization of the Coulomb interaction between charged particles (electron, holes, and lattice ions) in the vicinity of a plasmonic nanosystem is demonstrated for transitions resonant with SP eigenmodes in the nanosystem. There are three important features of this renormalized interaction $W(\mathbf{r}, \mathbf{r}'; \omega)$ that we have shown above and would like to reemphasize here. (i) This renormalization (enhancement) is highly resonant. Its phase depends on the frequency detuning of the electronic transitions with respect to the SP resonant frequency, changing by π (from in-phase to out-of-phase and *vice versa*) as frequency ω scans from the red to blue side of the SP resonance. (ii) The renormalized interaction $W(\mathbf{r}, \mathbf{r}'; \omega)$ is long-ranged: the effective interaction length is on the order of the size of the entire nanosystem. (iii) This renormalization and plasmonic enhancement of the Coulomb interaction is a universal effect, which should affect a wide range of physical phenomena in the vicinity of the metal nanoplasmonic systems: scattering between charge carriers and the carriers and ions, ion-ion interactions, exciton formation, etc. One of the enhanced and long-range phenomena, which is due to the nanoplasmonic renormalization of the Coulomb interaction, is the Förster energy transfer that becomes efficient for high-aspect ratio nanoshells.

Among other potentially very important applications of this theory are chemical reactions and catalysis on nanostructured metal surfaces. Chemical reactions occur due to the Coulomb interaction between charged particles (electrons and ions) at small distances. In many cases, nanostructured metals, in particular noble metal nanostructures with pronounced plasmonic behavior, are good catalysts. The results of this theory show that the Coulomb interaction at small distances is significantly renormalized. As we have emphasized in the previous paragraph, this renormalization is highly resonant depending on the frequency ω of a transition that controls the chemical transformation (for example, breaking a chemical bond, establishing a desired new bond, isomerization, etc.). This renormalization leads to suppression of the Coulomb interaction for the red detunings from the plasmonic resonance. In contrast, this local interaction is greatly enhanced for blue detunings from the SP resonance. This resonant effect opens up an avenue toward “designer” nanostructured catalysts that can, e.g., favor one specific reaction path over others. Another class of important effects, which are based on the nonlocal nature of the renormalized Coulomb interaction in the vicinity of a nanoplasmonic system, is the nonlocal (cross) scattering. A charge at some point can undergo a transition, scattering from a charge at a remote position, thus “teleporting” momentum and energy. One important instance of such a remote scattering is a nonlocal SERS where an electronic transition occurs at one point but the vibrational energy is deposited at a distant point of the nanoplasmonic system.

I. METHODS

A. Eigenproblem and Green’s Functions of Nanoplasmonic System

In this Section, for the sake of completeness and convenience, we outline obtaining Green’s function expressions within the framework of spectral theory^{6,18,20}. Consider a system consisting of a metal with dielectric permittivity $\varepsilon_m(\omega)$, dependent on optical frequency ω , embedded in a dielectric background with dielectric constant ε_h . The

geometry of the system is described by the characteristic function $\Theta(\mathbf{r})$, which equals 1 in the metal and 0 in the dielectric. Material properties of the system are described by the spectral parameter $s(\omega) = [1 - \varepsilon_m(\omega)/\varepsilon_h]^{-1}$.

For a nanosystem, which has all sizes much smaller than the relevant electrodynamic dimensions (radiation wavelength across the propagation direction of the excitation wave and the skin depth in this direction), the quasistatic approximation is applicable. In such a case, we define retarded Green's function $\bar{G}^r(\mathbf{r}, \mathbf{r}'; \omega)$ as satisfying the continuity equation with the δ -function right-hand side,

$$\left[\frac{\partial}{\partial \mathbf{r}} \Theta(\mathbf{r}) \frac{\partial}{\partial \mathbf{r}} - s(\omega) \frac{\partial^2}{\partial \mathbf{r}^2} \right] \bar{G}^r(\mathbf{r}, \mathbf{r}'; \omega) = \delta(\mathbf{r} - \mathbf{r}') \quad (7)$$

and homogeneous Dirichlet or Dirichlet-Neumann boundary conditions.

It is convenient to expand the Green's function over eigenmodes $\varphi_n(\mathbf{r})$ and the corresponding eigenvalues s_n that satisfy a homogeneous counterpart of Eq. (7)

$$\left[\frac{\partial}{\partial \mathbf{r}} \Theta(\mathbf{r}) \frac{\partial}{\partial \mathbf{r}} - s_n \frac{\partial^2}{\partial \mathbf{r}^2} \right] \varphi_n(\mathbf{r}) = 0, \quad (8)$$

with the homogeneous boundary conditions. This spectral expansion of the Green's function can be readily obtained from Eq. (7). It has an explicit form

$$\bar{G}^r(\mathbf{r}, \mathbf{r}'; \omega) = \sum_n \frac{\varphi_n(\mathbf{r}) \varphi_n(\mathbf{r}')}{s(\omega) - s_n}. \quad (9)$$

Two features of this expansion are important. First, it separates the dependencies on geometry and material properties. The geometrical properties of the nanosystem enter only through the eigenfunctions φ_n and eigenvalues s_n that are independent on the material properties of the system. Therefore they can be computed for a given geometry once and stored, which simplifies and accelerates further computations. Complementary, the material properties of the system enter Eq. (9) only through a single function: spectral parameter $s(\omega)$. The second important feature is that this Green's function satisfies exact analytical properties due to the form of Eq. (9) that contains only simple poles in the lower half-plane of the complex frequency ω and does not have any singularities in the upper half-plane of ω . Consequently, \bar{G}^r is a retarded Green's function that automatically guarantees the causality of the results of time-dependent calculations. Namely, the Green's function in time domain satisfies the condition $\bar{G}^r(\mathbf{r}, \mathbf{r}'; t) = 0$ for $t < 0$.

We introduce also another retarded Green's function G^r that is related to \bar{G}^r by an equation

$$\frac{\partial}{\partial \mathbf{r}} \Theta(\mathbf{r}) \frac{\partial}{\partial \mathbf{r}} \bar{G}^r(\mathbf{r}, \mathbf{r}'; \omega) = \frac{\partial^2}{\partial \mathbf{r}^2} G^r(\mathbf{r}, \mathbf{r}'; \omega). \quad (10)$$

Taking into account Eqs. (8)-(10), we immediately obtain for $G^r(\mathbf{r}, \mathbf{r}'; \omega)$ the eigenmode expansion given by Eq. (3). Dyadic Green's function $G_{\alpha\beta}^r$ and the corresponding dyadic renormalized potential $W_{\alpha\beta}$ are defined as

$$G_{\alpha\beta}^r(\mathbf{r}, \mathbf{r}'; \omega) = \frac{\partial^2}{\partial r_\alpha \partial r'_\beta} G^r(\mathbf{r}, \mathbf{r}'; \omega), \quad W_{\alpha\beta}(\mathbf{r}, \mathbf{r}'; \omega) = \frac{\partial^2}{\partial r_\alpha \partial r'_\beta} V(\mathbf{r} - \mathbf{r}') + \frac{4\pi}{\varepsilon_h} G_{\alpha\beta}^r(\mathbf{r}, \mathbf{r}'; \omega), \quad (11)$$

where $\alpha, \beta = x, y, z$.

B. Nonradiative and Radiative Relaxation of NQD in Proximity of Nanoplasmonic System

An important process, which can contribute to the linewidths γ_a and γ_d of the NQD donor and acceptor transitions, is the nonradiative transfer of energy from NQDs to a metal. The corresponding contribution to linewidths γ_m can be found in a straightforward way (cf. Ref. 31) to have the form

$$\gamma_m = -\frac{2\pi|\mathbf{d}|^2}{3\hbar\varepsilon_h} \text{Im} G_{\alpha\alpha}^r(\mathbf{r}, \mathbf{r}; \omega), \quad (12)$$

where \mathbf{d} is either \mathbf{d}_d or \mathbf{d}_a , and \mathbf{r} is the position of the NQD, which is considered as a point-like object.

Beside the FRET and the energy transfer to the metal (nonradiative relaxation), there is also a process of the radiative relaxation that can also be enhanced by the nanoplasmonic system (nanoantenna effect – see, e.g., Ref. 31).

The corresponding transition renormalized (SP-enhanced) dipole $\mathbf{d}^{(r)}$ and the radiative relaxation rate γ_r are given by

$$d_\alpha^{(r)} = d_\alpha + d_\beta \int \Theta(\mathbf{r}') G_{\alpha\beta}(\mathbf{r}, \mathbf{r}'; \omega) d^3 r' , \quad \gamma_r = \frac{4\omega^3}{3\hbar c^3} |\mathbf{d}^{(r)}|^2 , \quad (13)$$

where \mathbf{d} is the bare transition dipole.

C. Renormalized Coulomb Interaction for Nanoshells

For nanoshells, the eigenfunctions are given by products of the radial power functions and spherical harmonics that describe the angular dependence. The renormalized Coulomb potential $W(\mathbf{r}, \mathbf{r}'; \omega)$ for $r, r' > a$, where a is the external radius of the nanoshell, acquires the form

$$W(\mathbf{r}, \mathbf{r}'; \omega) = V(\mathbf{r} - \mathbf{r}') + \frac{4\pi}{\varepsilon_h a} \sum_{lm} \frac{F_l(x, \omega)}{2l+1} \left(\frac{a^2}{rr'}\right)^{l+1} Y_{lm}(\mathbf{r}) Y_{lm}^*(\mathbf{r}') . \quad (14)$$

Analogous expressions for the r and/or r' belonging to the inner part of the shell have also been obtained (not shown) and used in the computations, in particular, those illustrated in Fig. 2. In Eq. (14), the spherical harmonics Y_{lm} depend only on the directions of the corresponding vectors, and x is the shell aspect ratio (i.e., the ratio of the inner to outer shell radius). Form factor F_l is given by a resonant pole expression:

$$F_l(x, \omega) = \frac{s_l^+ f_l^+}{s(\omega) - s_l^+} + \frac{s_l^- f_l^-}{s(\omega) - s_l^-} , \quad (15)$$

where $P = \pm$ refers to symmetry of the corresponding SP mode and

$$f_l^\pm = \pm \frac{(\pm\lambda + 1)(2l + 1 \pm \lambda)}{4\lambda(l + 1)} , \quad s_l^\pm = \frac{l + (1 \mp \lambda)/2}{2l + 1} , \quad \lambda = \sqrt{1 + 4l(l + 1)x^{2l+1}} . \quad (16)$$

Note that SP eigenmodes with the $P = +$ symmetry have dominating oscillator strength in the long-wavelength (red and near-ir) part of the spectrum, where the quality factor of the SP resonances for noble metals is high, and which are most important in many cases.

D. FRET and Quenching Rates for NQDs on Nanoshell

We will calculate here the FRET rate $\bar{\gamma}_F$ averaged over the position of the acceptor on the nanoshell. Because we are interested in the SP-enhanced transfer over the distances much exceeding the usual Förster range, we will disregard the bare Coulomb potential $V(\mathbf{r} - \mathbf{r}')$. Then substituting the SP eigenfunctions and eigenvalues into Eq. (12) and integrating over the solid angle of the vector \mathbf{r}' , we obtain

$$\bar{\gamma}_F = \frac{2\pi |\mathbf{d}_a|^2 |\mathbf{d}_d|^2}{9\varepsilon_h^2 \hbar^2 a^6} J \sum_{l=1}^{\infty} |F_l(x, \omega)|^2 (2l + 1)(l + 1)^2 \left(\frac{a^2}{rr'}\right)^{2l+4} . \quad (17)$$

The rate γ_m of the excitation quenching due to the energy transfer to the metal on the nanoshell is obtained from Eq. (12) by the substitution of the SP eigenfunctions and eigenvalues. This procedure is actually greatly simplified, without affecting the result, if the angular averaging is performed. This leads to a simple expression

$$\gamma_m = -\frac{|\mathbf{d}|^2}{6\varepsilon_h \hbar a^3} \sum_{l=1}^{\infty} \text{Im} F_l(x, \omega) (2l + 1)(l + 1) \left(\frac{a}{r}\right)^{2l+4} . \quad (18)$$

This work was supported by grants from the Chemical Sciences, Biosciences and Geosciences Division of the Office of Basic Energy Sciences, Office of Science, U.S. Department of Energy, a grant CHE-0507147 from NSF, a grant from the US-Israel BSF, and by the DOE Center for Integrated Nanotechnologies jointly operated by the the Los Alamos and Sandia National Laboratories. MIS gratefully acknowledges useful discussions with D. Bergman and A. Nitzan.

Correspondence and requests for materials should be addressed to MIS (email: mstockman@gsu.edu)

-
- ¹ Fleischmann, M., Hendra, P. J. & McQuillan, A. J. Raman spectra of pyridine adsorbed at a silver electrode. *Chem. Phys. Lett.* **26**, 163–166 (1974).
 - ² Jeanmaire, D. L. & Van Duyne, R. P. Surface Raman spectroelectrochemistry part I. Heterocyclic, aromatic, and aliphatic amines adsorbed on the anodized silver electrode. *J. Electroanal Chem.* **84**, 1–20 (1977).
 - ³ Albrecht, M. G. & Creighton, J. A. Anomalously intense Raman spectra of pyridine at a silver electrode. *J. Amer. Chem. Soc.* **99**, 5215 – 5217 (1977).
 - ⁴ Kneipp, K. *et al.* Single molecule detection using surface-enhanced Raman scattering (SERS). *Phys. Rev. Lett.* **78**, 1667–1670 (1997).
 - ⁵ Hartschuh, A., Pedrosa, H. N., Novotny, L. & Krauss, T. D. Simultaneous fluorescence and Raman scattering from single carbon nanotubes. *Science* **301**, 1354–1356 (2003).
 - ⁶ Stockman, M. I. Electromagnetic theory of SERS. In Kneipp, K., Moskovits, M. & Kneipp, H. (eds.) *Surface Enhanced Raman Scattering – Physics and Applications*, 47–66 (Springer-Verlag, Heidelberg New York Tokyo, 2006).
 - ⁷ Lakowicz, J. R. Radiative decay engineering: Biophysical and biomedical applications. *Anal. Biochem.* **298**, 1–24 (2001).
 - ⁸ Shimizu, K. T., Woo, W. K., Fisher, B. R., Eisler, H. J. & Bawendi, M. G. Surface-enhanced emission from single semiconductor nanocrystals. *Phys. Rev. Lett.* **89**, 117401–1–4 (2002).
 - ⁹ Gerton, J. M., Wade, L. A., Lessard, G. A., Ma, Z. & Quake, S. R. Tip-enhanced fluorescence microscopy at 10 nanometer resolution. *Phys. Rev. Lett.* **93**, 180801–1–4 (2004).
 - ¹⁰ Kuhn, S., Hakanson, U., Rogobete, L. & Sandoghdar, V. Enhancement of single-molecule fluorescence using a gold nanoparticle as an optical nanoantenna. *Phys. Rev. Lett.* **97**, 017402–1–4 (2006).
 - ¹¹ Novotny, L. & Stranick, S. J. Near-field optical microscopy and spectroscopy with pointed probes. *Ann. Rev. Phys. Chem.* **57**, 303–331 (2006).
 - ¹² Dulkeith, E. *et al.* Gold nanoparticles quench fluorescence by phase induced radiative rate suppression. *Nano Lett.* **5**, 585–589 (2005).
 - ¹³ Ichimura, T., Hayazawa, N., Hashimoto, M., Inouye, Y. & Kawata, S. Tip-enhanced coherent anti-Stokes Raman scattering for vibrational nanoimaging. *Phys. Rev. Lett.* **92**, 220801–4 (2004).
 - ¹⁴ Kneipp, J., Kneipp, H. & Kneipp, K. Two-photon vibrational spectroscopy for biosciences based on surface-enhanced hyper-raman scattering. *Proc. Natl. Acad. Sci. USA* **103**, 17149–17153 (2006).
 - ¹⁵ Klimov, V. I. & McBranch, D. W. Femtosecond 1P-to-1S electron relaxation in strongly confined semiconductor nanocrystals. *Phys. Rev. Lett.* **80**, 4028–4031 (1998).
 - ¹⁶ West, J. L. & Halas, N. J. Engineered nanomaterials for biophotonics applications: Improving sensing, imaging, and therapeutics. *Annual Rev. Biomed. Eng.* **5**, 285–292 (2003).
 - ¹⁷ Achermann, M. *et al.* Energy-transfer pumping of semiconductor nanocrystals using an epitaxial quantum well. *Nature* **429**, 642–646 (2004).
 - ¹⁸ Stockman, M. I., Faleev, S. V. & Bergman, D. J. Localization versus delocalization of surface plasmons in nanosystems: Can one state have both characteristics? *Phys. Rev. Lett.* **87**, 167401–1–4 (2001).
 - ¹⁹ Stockman, M. I., Faleev, S. V. & Bergman, D. J. Coherent control of femtosecond energy localization in nanosystems. *Phys. Rev. Lett.* **88**, 067402–1–4 (2002).
 - ²⁰ Stockman, M. I., Bergman, D. J. & Kobayashi, T. Coherent control of nanoscale localization of ultrafast optical excitation in nanosystems. *Phys. Rev. B* **69**, 054202–1–10 (2004).
 - ²¹ Johnson, P. B. & Christy, R. W. Optical constants of noble metals. *Phys. Rev. B* **6**, 4370–4379 (1972).
 - ²² Förster, T. Zwischenmolekulare energiewanderung und fluoreszenz. *Ann. Phys.-Berlin* **437**, 55–75 (1948).
 - ²³ Dexter, D. L. A theory of sensitized luminescence in solids. *J. Chem. Phys.* **21**, 836–850 (1953).
 - ²⁴ Hua, X. M., Gersten, J. I. & Nitzan, A. Theory of energy transfer between molecules near solid state particles. *J. Chem. Phys.* **83**, 3650–3659 (1985).
 - ²⁵ Govorov, A. O., Lee, J. & Kotov, N. A. Theory of plasmon-enhanced Förster energy transfer in optically excited semiconductor and metal nanoparticles. *Phys. Rev. B* **76**, 125308–1–16 (2007).
 - ²⁶ Lakowicz, J. R. *et al.* Radiative decay engineering 2. Effects of silver island films on fluorescence intensity, lifetimes, and resonance energy transfer. *Anal. Biochem.* **301**, 261–277 (2002).
 - ²⁷ Andrew, P. & Barnes, W. L. Energy transfer across a metal film mediated by surface plasmon polaritons. *Science* **306**, 1002–1005 (2004).
 - ²⁸ Kagan, C. R., Murray, C. B., Nirmal, M. & Bawendi, M. G. Electronic energy transfer in CdSe quantum dot solids. *Phys. Rev. Lett.* **76**, 1517–1–4 (1996).
 - ²⁹ Crooker, S. A., Hollingsworth, J. A., Tretiak, S. & Klimov, V. I. Spectrally resolved dynamics of energy transfer in quantum-dot assemblies: Towards engineered energy flows in artificial materials. *Phys. Rev. Lett.* **89**, 1868021–4 (2002).
 - ³⁰ Achermann, M., Petruska, M. A., Crooker, S. A. & Klimov, V. I. Picosecond energy transfer in quantum dot Langmuir-Blodgett nanoassemblies. *J. Phys. Chem. B* **107**, 13782–13787 (2003).
 - ³¹ Novotny, L. & Hecht, B. *Principles of Nano-Optics* (Cambridge University Press, Cambridge, New York, 2006).